J. Fluid Mech. (1992), *vol.* 242, *pp.* 1–29
Printed in Great Britain

The dimension of attractors underlying periodic turbulent Poiseuille flow

By LAURENCE KEEFE[1]†, PARVIZ MOIN[2,3] AND JOHN KIM[3]

[1] Center for Turbulence Research, MS 202A-1, NASA-Ames Research Center, Moffett Field, CA 94035, USA

[2] Stanford University, Stanford, CA 94305, USA

[3] NASA-Ames Research Center, Moffett Field, CA 94035, USA

(Received 12 February 1991 and in revised form 17 January 1992)

Using a coarse grained ($16 \times 33 \times 8$) numerical simulation, a lower bound on the Lyapunov dimension, D_λ, of the attractor underlying turbulent, periodic Poiseuille flow at a pressure-gradient Reynolds number of 3200 has been calculated to be approximately 352. These results were obtained on a spatial domain with streamwise and spanwise periods of 1.6π, and correspond to a wall-unit Reynolds number of 80. Comparison of Lyapunov exponent spectra from this and a higher-resolution ($16 \times 33 \times 16$) simulation on the same domain shows these spectra to have a universal shape when properly scaled. Using these scaling properties, and a partial exponent spectrum from a still higher-resolution ($32 \times 33 \times 32$) simulation, we argue that the actual dimension of the attractor underlying motion on the given computational domain is approximately 780. The medium resolution calculation establishes this dimension as a strong lower bound on this computational domain, while the partial exponent spectrum calculated at highest resolution provides some evidence that the attractor dimension in fully resolved turbulence is unlikely to be substantially larger. These calculations suggest that this periodic turbulent shear flow is deterministic chaos, and that a strange attractor does underly solutions to the Navier–Stokes equations in such flows. However, the magnitude of the dimension measured invalidates any notion that the global dynamics of such turbulence can be attributed to the interaction of a few degrees of freedom. Dynamical systems theory has provided the first measurement of the complexity of fully developed turbulence; the answer has been found to be dauntingly high.

1. Introduction

Is the 'strange attractor' the underlying mathematical structure of fully developed turbulent shear flows? Despite nearly a century of theoretical and experimental research into the origins and development of fluid turbulence, the explicit mathematical framework that connects the chaotic, time-dependent dynamics of real flows to the structure of the Navier–Stokes (NS) equations has only recently begun to emerge. Nonlinear dynamical systems theory has laid claim to the candidacy for this framework, primarily as a result of its discovery and definition of that mathematical object called a 'strange attractor'. Such objects represent the solutions to differential equations, and carry within their intrinsic structure a well-defined mechanism (usually called 'sensitive dependence on initial conditions') that

† Current address: Nielsen Engineering & Research, 510 Clyde Ave., Mountain View, CA 94043, USA

can produce chaotic and unpredictable behaviour in all physical systems, without requiring random forcing. In addition to conjecturing that the strange attractor connects the NS equations and turbulence, dynamical systems theory has made itself attractive by predicting that turbulence is describable, asymptotically, by a finite number of degrees of freedom, despite the NS equations being infinite-dimensional. This has encouraged hope that the turbulence problem can be reduced in apparent complexity by projecting it onto some special basis. The general notion that a complex flow can be decomposed into low-dimensional subunits couples easily to previous ideas about the importance of coherent structures, and has animated a number of recent studies. Several have expanded on Lumley's (1981) suggestion that the Proper Orthogonal Decomposition, or Karhunen–Loéve procedure, is a rational way to extract such structures. Such an approach was used by Aubry *et al.* (1988), to characterize the near-wall dynamics in pipe flow, and by Sirovich & Rodriguez (1987) to obtain a low-dimensional description of chaotic solutions to the Ginzburg–Landau equation. In the former study the resulting 10-dimensional system of ordinary differential equations for the structure amplitudes displays an intermittency phenomenon that may be the essential mathematical model of 'bursting' in bounded shear flows. Moin & Moser (1989) performed the most complete such decomposition for Poiseuille flow, confirming that the most energetic 'characteristic eddy' was an ejection straddled by a pair of weak streamwise vortices. Sirovich, Ball & Keefe (1990) interpreted the decomposition in terms of plane waves in Poiseuille flow and conjectured a Reynolds-stress production scenario in which weak, obliquely propagating modes trigger activity in the energetic non-propagating modes. Independently of this decomposition approach, Jiminez & Moin (1991) used the versatility of numerical simulations to isolate a 'minimal' flow unit in near-wall turbulence consisting of a single time-varying low-speed streak. In a broader functional setting there is increasing theoretical proof (see references in Foias *et al.* 1988) that the solutions of several well-studied partial differential evolution equations (the two-dimensional Navier–Stokes equations included) possess global attractors to which all solutions are attracted, and that in some cases, these attractors are embedded in finite dimensional *inertial manifolds* in function space. On such manifolds their dynamics are formally representable by finite systems of ordinary differential equations. This result has not been rigorously established for the three-dimensional Navier–Stokes equations, but some version of it is certainly suggested by the fact that two evolution equations (Kuramoto–Sivashinsky, Ginzburg–Landau) derived from the Navier–Stokes do have this property.

The validity of dynamical systems theory as a descriptor of many supercritical fluid phenomena in Bénard convection and Taylor–Couette flow seems well established (Gollub & Benson 1980; Libchaber, Fauve & Laroche 1983; Gorman, Widmann & Robbins 1986; Moore *et al.* 1983; Busse 1981; Brandstater & Swinney 1987). Most importantly, the concept that the complicated dynamics of these fluid systems are attributable to the interactions of a rather small number of degrees of freedom has been validated.

Despite shear flow turbulence being regarded as the paradigm of chaos, dynamical systems theory has not yet found acceptance as the framework for turbulence in channels, jets, boundary layers, and wakes. In part this is because experimental verification has proven to be so much more difficult than in the Bénard and Taylor–Couette systems. In addition there remain substantial questions about the utility and descriptive power of the theory in situations where the flow is 'open' (convectively unstable) rather than 'closed' (absolutely unstable). Bénard con-

vection and Taylor–Couette flow are closed flows, and thus the global (collective) dynamics of the system are expressed at all spatial locations. In this situation the notion of an attractor on which these global dynamics reside is easy to grasp, since its phase-space basis can be quickly linked to familiar eigenmodes. In developing flows, such as boundary layers, jets and wakes, our intuitive notions tell us that local measurements do not express the global dynamics of the system, and defining its degrees of freedom is a subtler matter. In fact, definition of the 'system' itself is problematic for such flows, since their spatial domain can be arbitrarily large. Whether the collective dynamics of such a flow can be expressed using the notion of attractor is certainly unclear. Recent work by Abergel (1990) provides a proof that solutions to the forced, two-dimensional Navier–Stokes equation on an infinite strip $(-\infty, \infty) X[0, L]$ do possess a finite-dimensional, global attractor, if the forcing meets certain easily satisfied technical conditions. While there are technical problems to be overcome before this result can be extended to three-dimensional flows, it apparently encompasses the two-dimensional versions of jets, wakes, shear layers and boundary layers that are commonly studied and simulated. Thus there appears to be at least a theoretical basis for believing in the existence of attractors in developing flows. However, the practical aspects of defining their degrees of freedom, and thus the phase space in which their attractors are best envisioned, are undeveloped. This problem is eased, though not solved, by the realization that any real developing flow possesses a finite range of lengthscales, even if it is convenient to consider that it occurs on a semi-infinite domain.

For fully developed turbulence, such as turbulent Poiseuille flow, the question of 'closed' versus 'open', and that of describing its global dynamics has several subtleties. The label 'fully developed' implies that all statistical characteristics of the flow (and thus any chaotic dynamics) are unchanging in the flow direction. Imagine examining the flow inside a box which spanned the channel, and extended some arbitrary, but fixed amount, in the stream and cross-stream direction. One would expect to measure the same statistics and flow dynamics in it regardless of its position within the fully developed region. This translational invariance means that the global dynamics of the flow in the box are accessible from any point in the box. As noted before, this is one of the characteristics of a closed flow. On the other hand, Poiseuille flow is known to be convectively unstable (Huerre & Monkewitz 1985), and is thus, strictly speaking, an open flow. Similarly, the periodicity assumed in our flow simulation mathematically closes the flow, since disturbances convected out of one end of the computational domain are immediately convected back in on the upstream side (Poiseuille flow on a torus). This is certainly not characteristic of the real flow even in a closed-return wind tunnel, but extensive comparisons between experiments and simulation show that the latter accurately reproduces statistics, structures, and dynamical events measured in real flows. Thus the dynamical differences between this fully developed open flow and its simulated periodic counterpart are very subtle, even though the latter maintains an artificial correlation between flow quantities through its periodicity. It is certainly true that the simulations here do not possess the same range of scales as a real flow, but this is a matter of computational mechanics, not physics. Real duct flows (as well as jets, shear layers, wakes and boundary layers) do have both large- and small-scale cutoffs. It is only just beyond current computational capabilities to fully simulate a rectangular duct flow corresponding to available low-Reynolds-number experiments. Such a simulation might employ Chebyshev collocation or finite differences in both spanwise directions and periodic functions in the streamwise directions; thus it

would also be mathematically closed. Yet if current closed simulations with restricted scale ranges do an excellent job of predicting channel flow dynamics, how likely is it that a more complete simulation would do worse?

One concrete difference between a restricted-scale simulation and the real flow is the dimension of the underlying attractor. With scales restricted the attractor dimension in the simulation will be less than in the real flow. It has been repeatedly demonstrated in periodic simulations of the Kuramoto–Sivashinsky equation (Manneville 1985) and the Ginzburg–Landau equation (Sirovich, Rodriguez & Knight 1990; Keefe 1989) that the attractor dimension is an extensive property of the (computational) system size. This means that while the dimension of the attractor asymptotes to some fixed number as spatial resolution on a fixed domain is increased, that dimension would increase with system size provided the same high resolution were maintained on the new domain. Thus it is emphasized that the current results give the attractor dimension for periodic Poiseuille flow on a particular domain. Dividing by the streamwise and spanwise dimensions would then give a dimension per unit flow size that could be used to estimate the full dimension of any simulation on a larger domain or of an experimentally measured duct flow at the same Reynolds number. Since real flows have finite sizes, this implies that the dimension of the underlying attractor would also be finite.

It is in the context of the strong similarity between simulated and real Poiseuille flow, and the realization that the results must be scaled up to account for the larger, but finite domains of experiments, that we offer strong evidence that the mathematical structure of fully developed turbulence in a plane channel is characterized by an underlying strange attractor. At a single Reynolds number in turbulent channel flow we have determined a lower bound to the dimension, D_λ, of the underlying attractor on the given computational domain, having measured sufficient of the Lyapunov exponent hierarchy, λ_i, to calculate this quantity from the Kaplan–Yorke (Frederickson *et al.* 1983) definition:

$$D_\lambda = j + \frac{1}{|\lambda_{j+1}|}\sum_{i=1}^{i=j}\lambda_i, \tag{1.1}$$

where $\lambda_1+\lambda_2+\ldots+\lambda_j > 0$ and $\lambda_1+\lambda_2+\ldots+\lambda_{j+1} < 0$. This evidence is indirect in the sense that, while the existence of an attractor guarantees the existence of its Lyapunov exponents (Osledec 1968), calculation of a set of exponents using standard methods (Benettin *et al.* 1980) may not be the guarantee of an underlying attractor (though we are at a loss to say what else there could be). Traditional methods of visualizing attractors (Poincaré sections, maps) fail utterly for high-dimensional objects, so we have only the existence of a converged Lyapunov spectrum to infer the existence of an attractor. Such inference has been common in the past (Farmer 1982; Manneville 1985), and we employ it now. The Lyapunov exponents were calculated using standard methods (Benettin *et al.* 1980) except that the vectors separating solution trajectories were calculated in the phase space of the base trajectory rather than in its tangent space. Thus, only the Navier–Stokes equations were integrated, not these equations and their variational form. This alternative approach, equivalent to the standard one provided that the separation vectors are sufficiently small, has been used successively in the past (Keefe 1985) to determine the dimension of chaotic solutions to the Ginzburg–Landau equation, and was tested here over a range of separation vector sizes to demonstrate this equivalence.

There is previous work (Curry *et al.* 1984) in two- and three-dimensional simulations of Bénard convection showing that the asymptotic dynamics of such

simulations can be peculiarly sensitive to the spatial resolution of the calculation. There it was found that chaotic solutions at low resolution sometimes disappeared altogether as resolution increased. Because of this we have spent considerable effort to demonstrate that this 'return to order' does not occur in the turbulent channel, and that our coarse resolution results are a lower bound to the attractor dimension.

Dimension studies in several different flows have appeared following an earlier report of the current work (Keefe, Moin & Kim 1990). Kolmogorov flow was studied by Platt, Sirovich & Fitzmaurice (1991), while Sirovich & Deane (1991) examined low-Rayleigh-number chaotic Bénard convection. Grappin & Léorat (1991) studied forced two- and three-dimensional turbulence without shear. High dimensions were estimated or calculated for attractors in these latter two studies, but none so large as found here.

We first demonstrate the relative insensitivity of the Lyapunov spectra to changes in integration time step at fixed spatial resolution. What differences there are can be attributed to small changes in the total flow dissipation induced by discrete time integration. Next a calculation at increased spatial resolution shows that attractor dimension increases, but the Lyapunov exponent spectrum remains similar in shape when scaled by the number of non-negative exponents $N_{\geqslant}$ and the metric entropy h_{μ} (= sum of positive exponents). Assuming this scaling and shape similarity continue to hold as resolution increases, a third, partial spectrum calculation at still higher resolution provides evidence that the attractor dimension undergoes no further substantial growth.

Because dynamical systems theory predicts that the asymptotic behaviour of a dissipative dynamical system is confined to fewer degrees of freedom than needed to specify an initial condition, it has always been of interest to calculate the extent of this decrease. Calculating the dimension of the solution attractor supplies this information, for the dimension measures the number of degrees of freedom needed to characterize a point on the attractor in function space, and is a direct measure of the intrinsic complexity of the turbulence. Note that this complexity is quite different from the simpler spatial structure of turbulent fields that has been analysed in the context of multifractal sets by Meneveau & Sreenivasan (1987), and Prasad, Meneveau & Sreenivasan (1989). The context of that work is the Euclidean three-space of our daily experience, and thus all sets or objects there (such as the energy or scalar dissipation fields) require, at most, three degrees of freedom (coordinates) to describe them. The context of the current work is a high-dimensional ($\sim$ number of grid points $\times 2$ independent velocity components) function space in which an entire three-dimensional flow field at an instant is represented by a single point. The evolution of turbulent Poiseuille flow in time sweeps out a trajectory in this function space, and the current study attempts to determine the dimensionality of the set of points in that space that the flow visits as time becomes large.

Of the several definitions (Farmer, Ott & Yorke 1983; Grassberger & Procaccia 1983) of dimension available, we have chosen to use the Kaplan–Yorke formula (which bounds the fractal dimension (Constantin & Foias 1985)), since we have access to the dynamical equations (the NS equations) of the system, and can calculate the Lyapunov exponent hierarchy directly. This is in contrast to the two previous attempts (Sieber 1987; Brandstater, Swinney & Chapman 1986) to calculate the dimension of attractors in Poiseuille flow, that employed methods (time delay attractor reconstruction, correlation dimension) most suited to data derived from experiments. These attempts failed, the investigators concluding that the dimension is greater than 10 or 40 respectively. Because our calculations indicate that the

dimension is at least an order of magnitude greater than 40, we later argue that none of the 'experimental' methods for measuring dimension can be expected to work on this problem, because the data required exceeds current computer capabilities. This is true whether the method is a variant of the 'correlation' dimension (Grassberger & Procaccia 1983), or is one of the newer techniques (Eckmann & Ruelle 1985; Broomhead & King 1986; Wolf *et al.* 1985) to calculate the Lyapunov exponents experimentally.

2. The turbulent flow and its simulation

The geometry of turbulent Poiseuille flow is shown in figure 1. The flow conditions for which the dimension was calculated correspond to a Reynolds number R_p, based on constant pressure gradient ($= |\nabla p| L^3/2\rho\nu^2$, p = pressure, L = channel half-width, ρ = density, ν = kinematic viscosity), of 3200. In wall units, this yields a Reynolds number $Re_\tau = u_\tau L/\nu = 80$. This is below the value where the laminar parabolic flow becomes linearly unstable ($R_p = 5772$), and in the region ($R_p \approx 2900$) where it becomes unstable to finite-amplitude, two-dimensional disturbances. The major characteristics of the numerical method used to simulate the flow have been described by Kim, Moin & Moser (1987). It is spectral in all spatial directions, employing a complex exponential expansion in planes (x, z) parallel to the channel wall, and a Chebyshev polynomial expansion in the direction normal (y) to the channel wall. The time advance is of mixed character, employing explicit stepping for the nonlinear terms in the Navier–Stokes equations, and an implicit scheme for the viscous terms. The explicit scheme is now a compact storage third-order Runge–Kutta method devised by A. Wray at NASA Ames (private communication), rather than second-order Adams–Bashforth, but the implicit algorithm remains Crank–Nicholson.

Simulations were performed at three successively finer resolutions ($16 \times 33 \times 8$, $16 \times 33 \times 16$, $32 \times 33 \times 32$) on a spatial domain measuring $1.6\pi \times 2.0 \times 1.6\pi$ (x, y, z, all lengths scaled by L). Initial conditions for the coarse-grained simulation could be traced ultimately to spatially filtered versions of simulated fields at $Re_\tau = 180$ from Kim *et al.* (1987). The asymptotic turbulent flow field was then established (before the exponent calculation began) by advancing the flow for a time $tu_\tau/L = 276.28$. This corresponds to convection downstream at the mass-averaged velocity U_m for lengths of $6163L$. The exponent calculation, begun at this point, continued until $tu_\tau/L = 344.52$ ($7685L$). The flow simulation was further advanced until $tu_\tau/L = 497.74$ ($11\,103L$) to ensure that no unusual transients were contaminating the simulation, and that the central portion corresponding to the exponent calculation could be regarded as typical. The final condition of the coarse-grained simulation became the initial condition for the next higher resolution case ($16 \times 33 \times 16$). Starting from $tu_\tau/L = 0$ the flow was advanced until $tu_\tau/L = 253.58$ ($5080L$), from which point the exponent calculation extended till $tu_\tau/L = 326.1$ ($6535L$). A total time advance of $tu_\tau/L = 454.29$ ($9102L$) marked the end of calculations at this resolution. This final state again became the initial state for the next higher resolution calculation ($32 \times 33 \times 32$). Starting from zero this flow developed until $tu_\tau/L = 242.44$ ($4850L$), when exponent calculations extended until $tu_\tau/L = 250.42$ ($5010L$). A total time advance of $tu_\tau/L = 391.41$ ($7830L$) was achieved at this resolution. In each simulation we have gone to extraordinary lengths to ensure that the flow was in a statistically stationary state, all transients have died, and we are exponentially close to any attractor that may be there. The number of

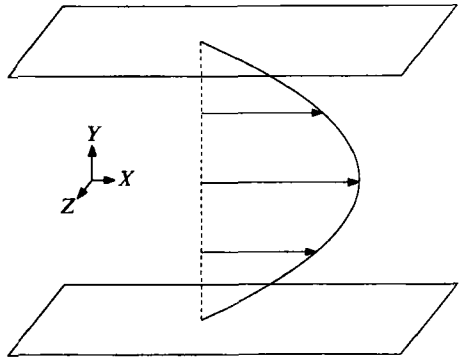

FIGURE 1. The geometry of turbulent Poiseuille flow.

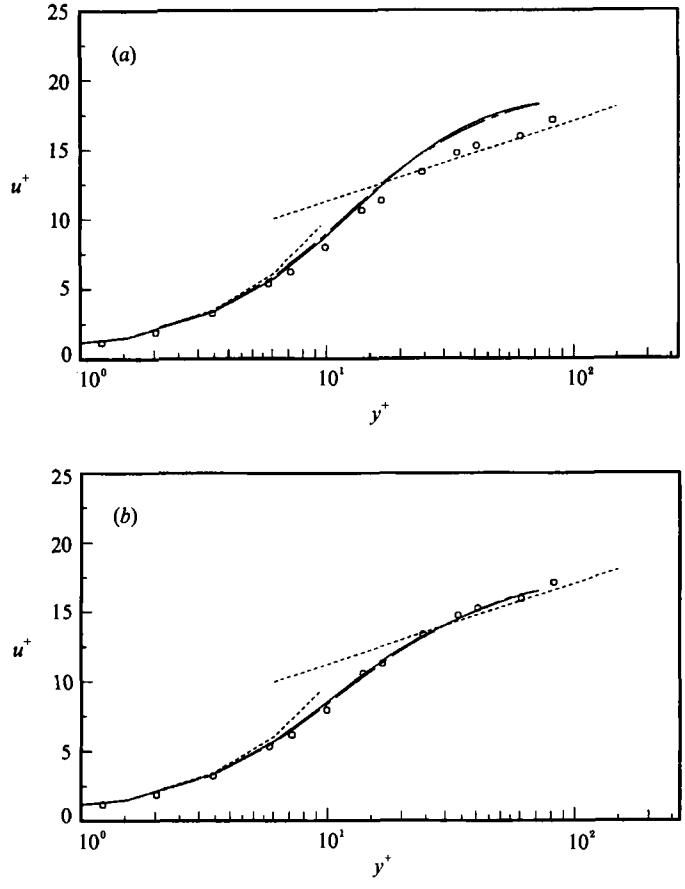

FIGURE 2. Near-wall velocity profiles $Re_\tau = 80$. (*a*) $16 \times 33 \times 8$ grid, (*b*) $16 \times 33 \times 16$ grid. ———, Upper wall; — — — —, lower wall; — — —, law of the wall. Symbols are the data of Eckelmann (1974).

convective lengthscales involved in each simulation exceeds by an order of magnitude that reported in any experimental work to date.

The Reynolds numbers of the three flows (coarse, medium and high resolution) based on mass-averaged velocity and channel half-width were 1190, 1069, and 1067. They were definitely chaotic and provided reasonable profiles of mean velocity,

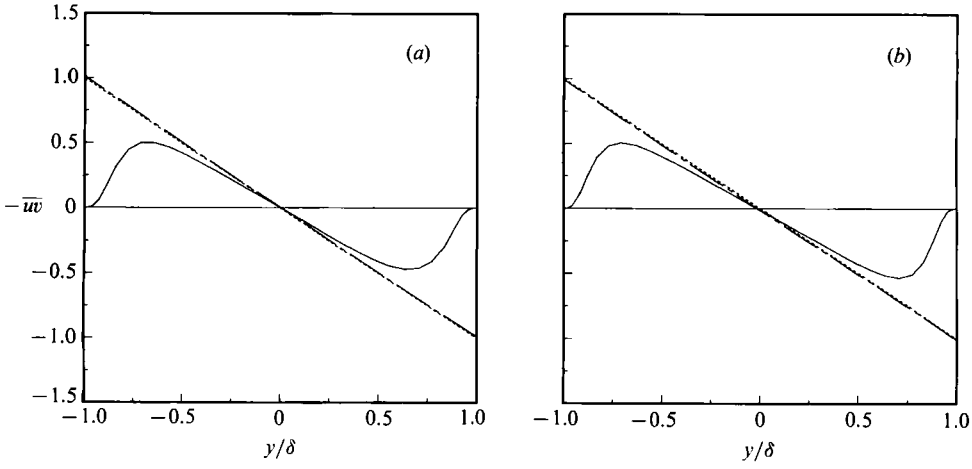

FIGURE 3. Stress distributions across the channel. (*a*) $16\times33\times8$ grid, (*b*) $16\times33\times16$ grid. ———, $\overline{u'v'}$; — — — —, $(1/Re)\partial U/\partial y-\overline{u'v'}$; — — —, total stress distribution in fully developed channel.

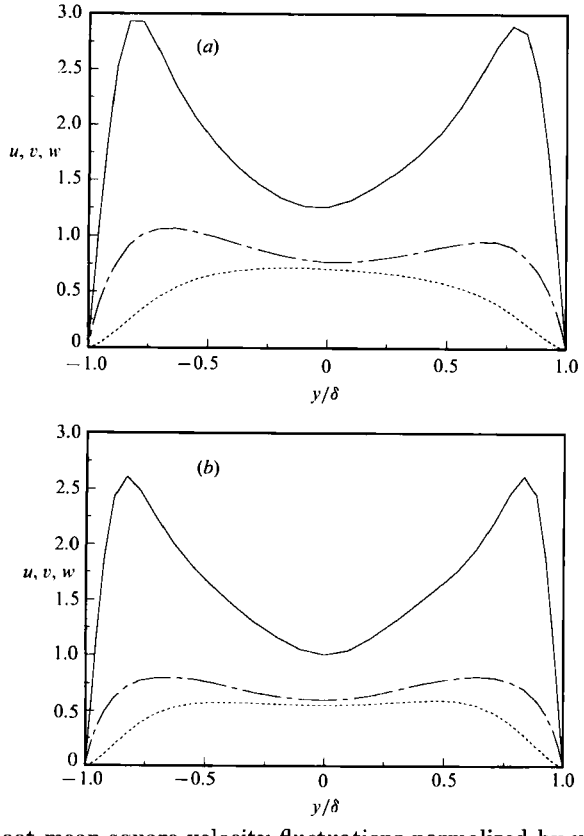

FIGURE 4. Root-mean-square velocity fluctuations normalized by wall shear velocity. (*a*) $16\times33\times8$ grid, (*b*) $16\times33\times16$ grid. ———, $u_{\rm rms}$; — — —, $v_{\rm rms}$; — — — —, $w_{\rm rms}$.

Reynolds stress and turbulence intensity across the channel. Do such simulations adequately model 'true' turbulence at these Reynolds numbers? Unfortunately there are no experimental data to compare to on turbulent channel flows in this low-Reynolds-number range, and the most accurate and well-resolved simulation (Kim

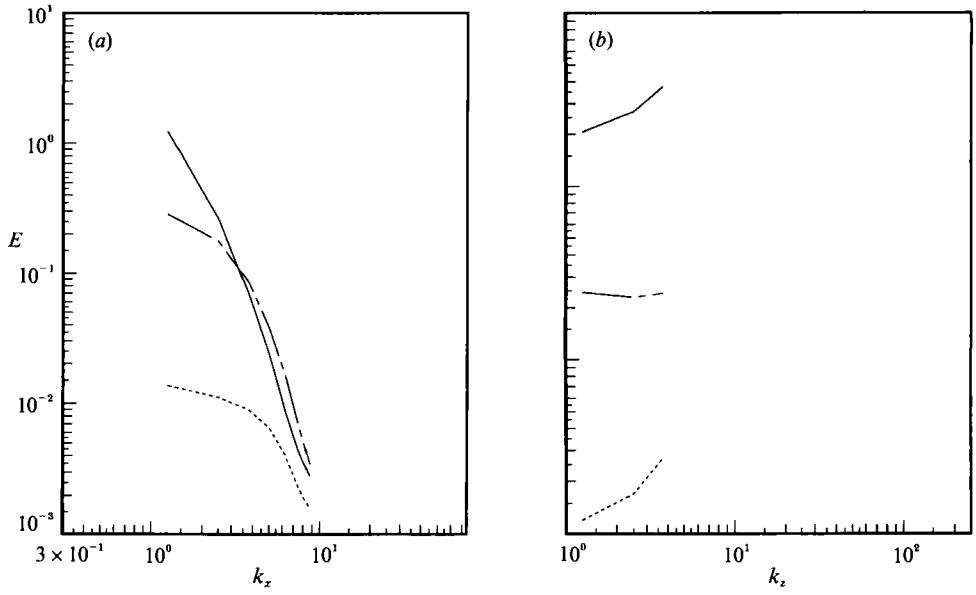

FIGURE 5. (*a*) Streamwise and (*b*) spanwise wavenumber spectra at $y^+ = 13.5$, $16\times33\times8$ grid. ———, u; — — —, v; — — — —, w.

et al. 1987) is at a mass-averaged Reynolds number of 2800. In figures 2–4 we show near-wall velocity profiles, Reynolds and total stress distribution across the channel and intensity profiles for the coarse and medium resolution simulations. Despite the fact that law-of-the-wall behaviour is not necessarily to be expected at low Reynolds numbers, the simulations show something fairly close, and the agreement improves with increased resolution. The symbols in figure 2 are the data of Eckelmann (1974), as corrected by Kim *et al.* (1987). The total stress distribution $(1/Re)\,\partial U/\partial y - \overline{u'v'}$ is linear from wall to wall in all simulations, though the peak of the Reynolds stress curve gets slightly larger and closer to the wall as resolution increases. Turbulent intensity profiles show the widest variation. Spanwise (w') and normal (v') fluctuations have the shape, though not the amplitude, of those found at higher Reynolds numbers, while longitudinal fluctuations (u') peak in the region $15 \leqslant y^+(= u_\tau y/\nu) \leqslant 20$ and have both the amplitude and shape expected.

Representative streamwise and spanwise wavenumber spectra at $y^+ = 13.5$ are shown in figures 5 and 6 for the lowest- and medium-resolution calculations. The primary differences are in the spanwise (k_z) spectra. These increase in amplitude with wavenumber at the lowest resolution, but peak and begin to fall off at the medium resolution. In the highest-resolution simulation the fall off simply extends to higher wavenumbers.

Grappin & Léorat (1991) have questioned whether simulations at even the highest resolution used here can be sufficiently dissipative for the dynamics, and thus the Lyapunov exponents and dimension, to be correct. We would have to agree that the lowest-resolution calculation does suffer from the lack of dissipation in spanwise motions. The resulting flow is too energetic. However, the first increase in spanwise resolution seems to go a long way towards correcting this problem. The mass-averaged velocity drops 10% with the first doubling of spanwise resolution, but remains unchanged by further resolution increases in both streamwise and spanwise directions. Note also that turbulent intensity profiles decrease in peak amplitude

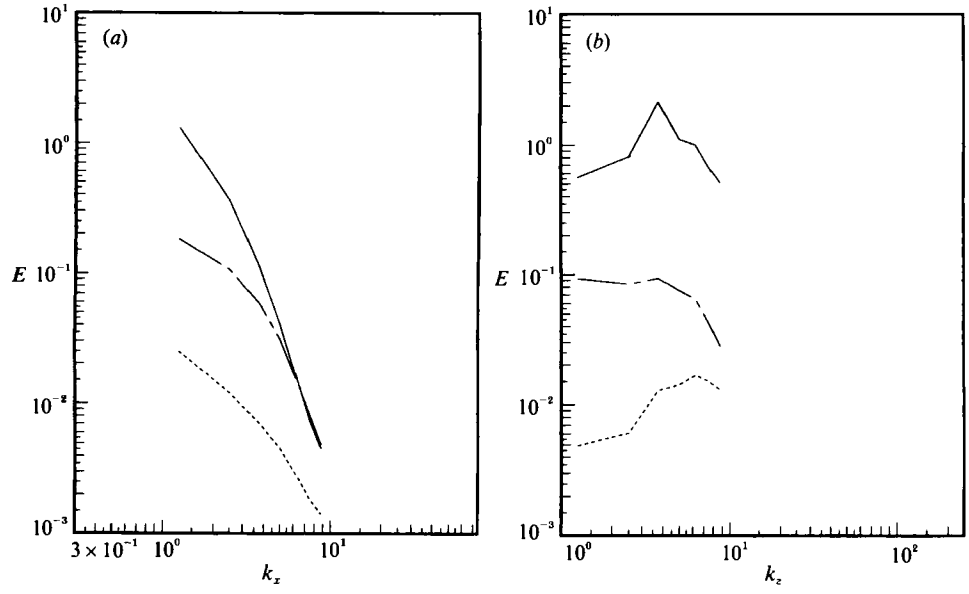

FIGURE 6. (a) Streamwise and (b) spanwise wavenumber spectra at $y^+ = 13.5$, $16 \times 33 \times 8$ grid. ———, u; — — —, v; ——— · ———, w.

much more with the first resolution increase than with the next. At medium resolution the grid spacing in terms of wall units was $\Delta x^+ = 25.2 = \Delta z^+$. The highest-resolution simulation halves these numbers to 12.6. These latter spacings are very similar to those found in the simulation of Kim *et al.* (1987), where all essential scales of motion were resolved (and this at a higher Reynolds number ($Re_\tau = 180$) than calculated here). What the current simulations lack are low, not high, wavenumber content, and this is unlikely to manifest itself as a lack of dissipation. The evidence suggests that the initial increase in spanwise resolution brings the simulation close to the asymptotic high-resolution flow and that some of the bulk flow quantities have already reached it. Rozhdestvensky & Simakin (1984) found similarly good bulk properties with low-resolution simulations in this same Reynolds-number range. None of these simulations may be 'true' turbulence, but the deviations from this state at medium and highest resolution seem unlikely to be important qualifications to the calculated Lyapunov exponents and attractor dimensions.

3. Lyapunov exponent calculation technique, and a test case

3.1. *Lyapunov exponents*

The Lyapunov exponents and vectors of a dynamical system measure the local expansion or contraction (exponents) of phase-space volume along particular directions (vectors) near the solution attractor of such a system. Consider a dynamical system in R^N

$$\frac{d\boldsymbol{X}}{dt} = f(\boldsymbol{X}), \quad \boldsymbol{X} \in R^N \tag{3.1}$$

and write its solution for a particular initial condition $\boldsymbol{X}(0) = \boldsymbol{X}_0$

$$\boldsymbol{X}(t) = \phi_t(\boldsymbol{X}_0). \tag{3.2}$$

The behaviour of infinitesimal perturbations $\delta \boldsymbol{X}(t)$ may be studied through the assumption

$$\boldsymbol{X}(t) = \phi_t(\boldsymbol{X}_0) + \delta \boldsymbol{X} \tag{3.3}$$

and linearization of (3.1) about $\phi_t(\boldsymbol{X}_0)$. This yields

$$\frac{\mathrm{d}\delta \boldsymbol{X}}{\mathrm{d}t} = Df[\phi_t(\boldsymbol{X}_0)]\,\delta \boldsymbol{X}, \tag{3.4}$$

where $Df[\ ]$ denotes the Jacobian matrix $[\partial f_i/\partial x_j]$, evaluated along the original trajectory $\phi_t(\boldsymbol{X}_0)$. Write the solution of this non-autonomous system (3.4) for a particular initial condition $\delta \boldsymbol{X}(0) = \delta \boldsymbol{X}_0$ as

$$\delta \boldsymbol{X}(t) = \mathrm{d}\phi_t^{\boldsymbol{X}_0}(\delta \boldsymbol{X}_0). \tag{3.5}$$

Thus $\delta \boldsymbol{X}_0$ is the initial separation vector between two nearby solution trajectories of the dynamical system (3.1) and $\delta \boldsymbol{X}(t)$ is their time varying separation.

Instead of one separation vector $\delta \boldsymbol{X}_0$, consider p independent initial separation vectors $\boldsymbol{V}_1, \boldsymbol{V}_2, \ldots \boldsymbol{V}_p$ chosen around $\boldsymbol{X}_0$ with $1 \leqslant p \leqslant N$. They define a p-dimensional parallelepiped in the p-dimensional subspace E^p of R^N. Call $\mathrm{Vol}_p(\boldsymbol{V}_1, \boldsymbol{V}_2, \boldsymbol{V}_3 \ldots \boldsymbol{V}_p)$ the p-dimensional volume of this parallelepiped. Under suitable assumptions (Benettin *et al.* 1980), one can define the *p-dimensional Lyapunov exponents*

$$\lambda^p(\boldsymbol{X}_0) = \lim_{t\to\infty} \frac{1}{t} \ln \left\{ \frac{\mathrm{Vol}_p[\mathrm{d}\phi_t^{\boldsymbol{X}_0}(\boldsymbol{V}_1), \ldots, \mathrm{d}\phi_t^{\boldsymbol{X}_0}(\boldsymbol{V}_p)]}{\mathrm{Vol}_p[\boldsymbol{V}_1, \boldsymbol{V}_2, \boldsymbol{V}_3 \ldots \boldsymbol{V}_p]} \right\}. \tag{3.6}$$

The $\mathrm{d}\phi_t(\boldsymbol{V}_i)$, etc. are the sides of the evolved parallelepiped. $\lambda^p(\boldsymbol{X}_0)$ represents the average expansion or contraction rate of infinitesimal p-volume near the solution attractor. Thus λ^1 describes the average behaviour of lengths, λ^2 the behaviour of areas, etc. For most chaotic attractors the λ^p are independent of $\boldsymbol{X}_0$.

The one-dimensional Lyapunov exponents λ_i are defined by

$$\left.\begin{aligned} \lambda_1 &= \lambda^1, \\ \lambda_i &= \lambda^i - \lambda^{i-1}. \end{aligned}\right\} \tag{3.7}$$

One generally speaks of the λ_i as *the* Lyapunov exponents of the system. They represent the average rate of expansion or contraction of lengths along a time-varying, but mutually orthogonal set of directions in the phase space near the attractor. These directions, called Lyapunov vectors, are not known *a priori*, but are themselves calculated on a time-varying basis as a precursor to determining the exponents. Their spatial form carries the structural information describing the kinds of perturbations to which a flow is most sensitive. Vastano & Moser (1991) have examined the first few Lyapunov vectors in Taylor–Couette flow near its transition to chaos, and shown how this transition stems from the instability of outflow jets produced by pairs of wavy vortices just below the transition.

The analogy between Lyapunov exponents and their associated vectors, and the eigenvalues and eigenmodes of stability theory should be apparent. However, it is only an analogy; Lyapunov exponents and vectors are not rigorous time-varying generalizations of the eigenvalues and eigenvectors of even an *undynamical* system ($\mathrm{d}\boldsymbol{X}/\mathrm{d}t = 0$ in (3.1)). In this case (3.4) describes perturbations to a fixed point(a steady solution to the Navier–Stokes equation, say). The Jacobian matrix $Df[\ ]$ is steady, and the usual normal mode analysis of this problem (e.g. for parallel flows, the Orr–Sommerfeld equation) is solved by determining the eigenvalues and eigenvectors of $Df[\ ]$. The eigenvalues of such an analysis have both an exponential and a fluctuating part. However, by definition, Lyapunov exponents measure

average growth or decay, not fluctuation. For steady flows the Lyapunov vectors and eigenmodes coincide, and it is apparent that in any long-time average of perturbative behaviour along such directions, the dependence on the fluctuating part of the eigenvalue disappears. In this special case the Lyapunov exponents equal the non-fluctuating parts of the eigenvalues of the Jacobian matrix (we are ignoring the case of eigenvalues of multiplicity greater than one). This fact can be used (Keefe 1985) to test the general validity of numerical techniques developed to determine the exponents of a particular dynamical system. Stability eigenvalues can be calculated by means independent of the Lyapunov exponent algorithm described below, thus an independent check of the exponents and vectors is possible. An alternative way to check an exponent calculation requires that the total dissipation of the dynamical system be known, and that the entire exponent spectrum be calculated. Then the sum of all the exponents should equal the total dissipation. In the case of the Lorenz equations the dissipation is known analytically, and this fact was used by Shimada & Nagashima (1979) to check their calculation of the dimension of the attractor for that system. In a similar fashion Yamada & Ohkitani (1988) were able to check their dimension results for a large system of equations derived from the Navier–Stokes equation, because here also the dissipation was known analytically. For direct simulation of Navier–Stokes turbulence this technique has limited usefulness, for an independent calculation of the dissipation is usually not available, nor is it usually possible to calculate all the exponents of even a coarse-grained simulation. The exception is integration of the forced Euler equations, for in this case the dissipation is zero and extremely coarse-grained simulations display chaotic behaviour. Grappin & Léorat (1991) used this device to check their exponent algorithm, later applied to forced incompressible Navier–Stokes turbulence.

The dissipation test, along with the stability technique employed here, provides only an algorithmic check; when dealing with discrete time integration there is an additional complication. Faced with a system of unknown dissipation, a good algorithm can be expected to estimate exponents consistent with that dissipation. But the dissipation of a discretely integrated dynamical system varies with the time step used, and so also do the estimated exponents and dimension. This phenomenon was found in the current simulations; we will later use the Lorenz system to demonstrate it analytically and to quantify its magnitude.

The basic details of the method employed to calculate the Lyapunov exponents of Poiseuille flow can be found in Shimada & Nagashima (1979) or Benettin *et al.* (1980). For a more expository description see Grappin & Léorat (1991) and Sirovich & Deane (1991). To compute M exponents the evolution of M initially orthogonal perturbations from the basic flow are followed for a short time and then reorthogonalized using a modified Gram–Schmidt procedure. At the time of reorthogonalization the relative exponential growth or decrease of the perturbations with respect to their initial amplitude is measured. Then the amplitudes of the new orthogonal ensemble of perturbations are normalized to some initial value and their evolution followed again. At each orthogonalization a local value of growth or decay exponent is recorded for each perturbation. When all the local values, for a given perturbation vector, are averaged after many orthogonalizations, the result is a Lyapunov exponent. The set of such numbers from all the perturbations is called the Lyapunov spectrum.

There are two different ways to follow perturbations of a dynamical system. The first way is to derive the variational equations of the system, and then advance unity norm perturbations under its influence, calculating the system coefficients from the

Mode no.	n	m	ω_i	ω_r	Mode type
1	0	0	−0.0725706	0	EH
2	0	1	−0.1019823	0	ES
3	0	2	−0.1902177	0	ES
4	1	0	−0.2521302	4.00046	ES
5	0	1	−0.2739335	0	ETS
6	1	1	−0.2815419	4.00046	ES
7	0	0	−0.2902825	0	OH
8	0	2	−0.2986788	0	ETS
9	0	1	−0.3196942	0	OS
10	0	3	−0.3372765	0	ES
11	2	0	−0.3609015	8.1464	ES
12	1	2	−0.3697772	4.00046	ES
13	2	1	−0.3903133	8.1464	ES
14	0	2	−0.4079295	0	OS
15	0	3	−0.4080372	0	ETS
16	3	0	−0.4495583	12.3169	ES
17	2	2	−0.4785486	8.1464	ES
18	3	1	−0.4789700	12.3169	ES
19	1	2	−0.5070494	27.9369	ETS
20	1	3	−0.5168360	4.00046	ES
21	4	0	−0.5294114	16.4999	ES
22	0	4	−0.5431589	0	ES
23	0	3	−0.5549883	0	OS

TABLE 1. Stability eigenvalues from Orr–Sommerfeld analysis at $R_p = 578$ ($Re_\tau = 34$). The final column refers to the type of mode and its symmetry across the channel: H, Heat; TS, Tollmien–Schlicting; S, Squire; E, even; O. odd.

time-varying state of the basic flow. In the second way the evolution of perturbations is constructed from monitoring the evolution of a family of initial conditions near the basic flow. The latter technique will provide the same answers as the former provided the initial separations between members of the family are small enough to make calculating neighbouring trajectories a good approximation to linearization. We have chosen the second approach, because it seemed to provide a slightly less complex implementation in programming. The core of the algorithm was a flow solver written to perform full numerical simulation of low-Reynolds-number channel flow (Kim *et al.* 1987). It has been tested and used extensively, demonstrating an ability not only to reproduce experimental results, but to go beyond them in elucidating flow features not easily investigated in experiments. In hindsight the perceived complexity of the other technique was probably more imagined than real, and it is to be preferred from the standpoint of round-off errors associated with small differences between large numbers. However, the exponent results presented in the remainder of the paper have been tested for independence with respect to changes in perturbation magnitude from 0.001 to 0.01. As the next subsection shows, this magnitude range produces exponents in excellent agreement with stability exponents calculated by solution of the Orr–Sommerfeld equation at a subcritical Reynolds number of $R_p = 578$.

3.2. *Test case*: *Poiseuille flow at* $R_p = 578$ ($Re_\tau = 34$)

The stability of laminar Poiseuille flow has been extensively documented by numerical means. Its linear instability occurs at $R_p = 5772$ (Orszag 1971), while the work of Herbert (1977) and others shows it stable to finite two-dimensional

disturbances for $R_p < 2800$. Rozhdestvensky & Simakin (1984) claim that the flow is nonlinearly stable to three-dimensional disturbances for $R_p < 2100$. Our own numerical simulations suggest that the three-dimensional nonlinear stability limit is closer to $R_p = 2300$. However, there can be no doubt that the flow is completely stable at $R_p = 578$ ($Re_\tau = 34$) where we have conducted a test of the Lyapunov exponent algorithm.

The full temporal linear instability equations for Poiseuille flow were solved using the Chebyshev tau method. Perturbation eigenfunctions

$$f_j(y)\,(u_j(x,y,z,t) = f_j(y)\exp(in\alpha x + im\beta z - i\omega t))$$

were expanded in the first 45 Chebyshev polynomials and the resulting eigenvalue problem for the complex frequency $\omega = \omega_r + i\omega_i$ solved by the IMSL routine EIGCC. The computational domain had fundamental streamwise and spanwise wavenumbers of $\alpha = 0.25$ and $\beta = 1$ respectively. The algorithm calculates both Tollmien–Schlicting waves and Squire modes and orders them from least to most stable. The first 23 eigenvalues are listed in table 1 along with the two 'heat conduction' modes ($n = m = 0$) whose analytically calculated decay rates ($\sigma_1 = -l^2\pi^2/4Re_\tau$) fall within the hierarchy. All frequencies and growth rates are presented in terms of the non-dimensional time tu_τ/L. To obtain rates based on centreline velocity scaling these results should be divided by $(\frac{1}{2}Re_\tau)^{\frac{1}{2}}$. It can be seen that a heat mode is the least stable, followed by two spanwise-propagating Squire modes. The least-stable streamwise-propagating TS wave is nineteenth in the hierarchy. These results are invariant to six decimal places for expansion of the eigenfunctions into 30 or more Chebyshev polynomials.

The exponent test calculation was conducted on a $16 \times 33 \times 16$ grid distributed within a computational domain $8\pi \times 2\pi$ in the streamwise and spanwise directions. The attractor, or central trajectory, whose exponents were calculated was steady, laminar Poiseuille flow $U(y) = (Re_\tau/2)(1-y^2)$. The initial set of 60 mutually orthogonal vectors of magnitude $\epsilon = 0.001$ separating the fixed point from the other initial conditions was produced by a random number generator. The orthonormalization interval was set to $\Delta tu_\tau/L = 0.05$. There is a considerable transient period during which the entire ensemble of separations relaxes toward its asymptotic state. The variation of the local exponent values during this period can be included in the long-time averages, but this markedly decreases their convergence rate. It is better to ignore variations during the transient period and only begin averaging when the separation vectors have reached their asymptotic orientation. The averages then converge very rapidly. Modes with $\omega_r = 0$ (no fluctuation, just decay) can be used to determine the end of the transient. When this point is reached the local exponent values will be unchanging from interval to interval. For the test case, mode 23 of table 1, an odd Squire mode with three spanwise wavelengths, was used for this purpose.

The first 60 Lyapunov exponents of laminar Poiseuille flow at $R_p = 578$ are presented in table 2. Both the magnitude and ordering of exponents can be checked by comparison to the column headed ω_i in table 1. The multiplicity with which a given exponent appears depends on the mode obliquity and possible $\frac{1}{2}\pi$ phase shifts in space. Such multiplicity does not reflect any multiplicity in the Orr–Sommerfeld eigenvalue problem. For oblique modes there are four mutually orthogonal disturbances with the same exponent. They are any two waves with $\alpha_2 = \alpha_1$, $\beta_2 = \beta_1$ and a $\frac{1}{2}\pi$ phase shift between them along the wave vector, and any two waves $\alpha_2 = \alpha_1$, $\beta_2 = -\beta_1$ with an arbitrary phase shift between them. Spanwise ($n = 0$) or stream-

Index, i	λ_i	Mode no.	Index, i	λ_i	Mode no.
1	−0.0725706	1	31	−0.3905574	13
2	−0.0725706	1	32	−0.3905575	13
3	−0.1019824	2	33	−0.4080372	15
4	−0.1019824	2	34	−0.4080373	15
5	−0.1902177	3	35	−0.4079297	14
6	−0.1902177	3	36	−0.4079297	14
7	−0.2521495	4	37	−0.4506828	16
8	−0.2521495	4	38	−0.4506828	16
9	−0.2739335	5	39	−0.4788416	17
10	−0.2739335	5	40	−0.4797154	17
11	−0.2815625	6	41	−0.4788354	17
12	−0.2815625	6	42	−0.4789766	17
13	−0.2815627	6	43	−0.4795453	18
14	−0.2815626	6	44	−0.4800679	18
15	−0.2903747	7	45	−0.4796223	18
16	−0.2932270	7	46	−0.4800910	18
17	−0.2957793	8	47	−0.5070506	19
18	−0.2985416	8	48	−0.5070504	19
19	−0.3196944	9	49	−0.5070506	19
20	−0.3196956	9	50	−0.5070504	19
21	−0.3372752	10	51	−0.5168686	20
22	−0.3372765	10	52	−0.5168686	20
23	−0.3611437	11	53	−0.5168688	20
24	−0.3611486	11	54	−0.5168687	20
25	−0.3697908	12	55	−0.5328953	21
26	−0.3698025	12	56	−0.5430818	22
27	−0.3698021	12	57	−0.5329181	21
28	−0.3698023	12	58	−0.5431173	22
29	−0.3905573	13	59	−0.5549936	23
30	−0.3905576	13	60	−0.5549944	23

TABLE 2. First 60 Lyapunov exponents at $R_p = 578$ ($Re_\tau = 34$)

wise ($m = 0$) modes are characterized by double exponents. They correspond to a wave and its $\frac{1}{2}\pi$-shifted image. The heat modes are special cases ($n = m = 0$). Here u and w independently satisfy the same diffusion equation. Thus one mode has u and not w, and the other has w and not u.

The general agreement between exponent values predicted by the Orr–Sommerfeld equation and the exponent algorithm is very good. The worst error in value is 1.01 % (for the second heat mode), multiplicities are correct, and there are only slight anomalies in ordering (Mode 15 before Mode 14, Mode 21 and Mode 22 interleaved) which occur when the predicted values of two exponents are very close to each other. The agreement between values often extends to four or more decimal places. Thus the comparison test gives us a high level of confidence in the Lyapunov exponent spectra of turbulent Poiseuille flow described in the next section. Errors of value and ordering such as found in the test case will have negligible effect on the shape of these spectra, as well as the value of dimension calculated from them using (1.1), the Kaplan–Yorke formula.

4. Lyapunov spectra and the dimension of the attractor

Four different Lyapunov exponent spectra were calculated for turbulent Poiseuille flow at $R_p = 3200$. The first two used the same coarse-grained spatial resolution ($16 \times 33 \times 8$), but different time steps ($\Delta t u_\tau / L = 0.0015,\ 0.003$) to integrate the Navier–Stokes equations. From both of these calculations sufficient of the Lyapunov spectrum was obtained to directly calculate the dimension of the underlying attractor using the Kaplan–Yorke formula. The remaining two exponent spectra were obtained at successively finer spatial resolutions ($16 \times 33 \times 16$, $32 \times 33 \times 32$) to investigate the dependence of the attractor dimension on resolved scale. Because of the increased computational effort involved, less of the spectra were obtained in these cases from the available computer resources. However, the results from the medium-resolution calculation were sufficient to confirm a scaling relation amongst spectra at different resolutions that allowed attractor dimension to be estimated at this and the most highly resolved flow condition. The overall result is simply stated: for the given computational domain and Reynolds number, a lower bound to the dimension of the underlying attractor was calculated to be $D_\lambda = 352$; doubling the spanwise resolution caused the estimated dimension to rise to $D_\lambda \approx 780$. The evidence suggests that a further doubling of both spanwise and streamwise resolution leaves this estimated dimension unchanged. However, this last statement must be hedged about by qualifiers, owing to the relatively small segment of the spectrum that could be calculated. We conclude the $D_\lambda \approx 780$ is a lower bound to the dimension of the strange attractor underlying turbulent Poiseuille flow on the given computational domain, and that there is evidence to support the contention that its asymptotic value for fully resolved turbulence is not substantially larger. Details of the individual calculations follow.

4.1. *Coarse-grained spatial resolution*

Two exponent spectra, differing only by the integration time step $\Delta t u_\tau / L$ used to obtain them, were calculated at the $16 \times 33 \times 8$ resolution. The primary results are displayed in figure 7, where the values of the Lyapunov exponents λ_i are plotted against their index i. For simulation at each time step the first 450 exponents were calculated, at a total cost of some 800 h of cpu time on a CRAY-2. Application of the Kaplan–Yorke formula to each distribution yields dimension estimates of $D_\lambda \sim 352$ ($\Delta t u_\tau / L = 0.0015$) and $D_\lambda \sim 308$ ($\Delta t u_\tau / L = 0.003$). The number of positive exponents is 166 and 142 respectively, and the metric entropies associated with these positive exponents are $h_\mu \sim 90$ and $h_\mu \sim 70$. The exponents with the higher indices converge most rapidly, and a strategy which averages the low-index exponents close to convergence, before adding additional trajectories to the ensemble to calculate the high-index exponents, makes most efficient use of computational time. After initial transients the first 63 exponents of the $\Delta t u_\tau / L = 0.0015$ (0.003) case were averaged for timescales corresponding to convection over $1427L$ ($1359L$). Exponents 64–250 were obtained from averages over the latter $730L$ ($541L$) of this period, exponents 251–450 from averages over the latter $470L$ ($338L$). Despite these long averaging times the exponent values are not strictly decreasing, and some small non-uniformities continue to persist at the boundaries between the averaging groups. These departures from ideal spectra have negligible effect on the dimension estimates.

Though the computational grid is $16 \times 33 \times 8$, and there are three velocity components at each node, particular features of the flow solver reduce the free nodes

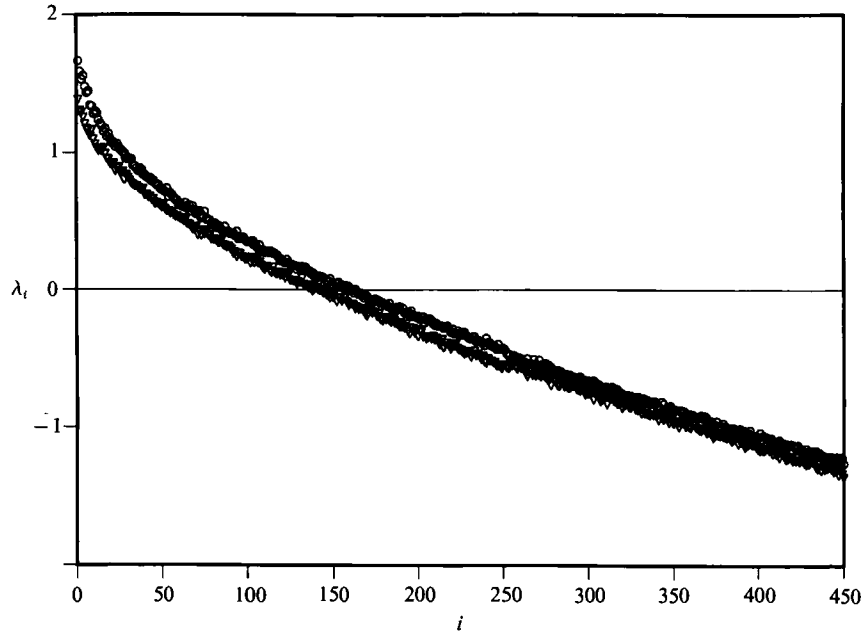

FIGURE 7. Distribution of Lyapunov exponents, λ_i for coarse-grained simulations of turbulent Poiseuille flow. ○, Time step 0.0015; ▽, time step 0.003.

to $15 \times 33 \times 7$, and incompressibility of the flow means that only two of the velocity components are independent; thus there are $15 \times 33 \times 7 = 6390$ degrees of freedom in the calculation, and the estimated dimensions are roughly 4–5% of the dimension of the complete phase space.

The simple fact that converged exponent spectra were obtained which yield dimension estimates substantially less than that of the phase space is strong evidence that an attractor ('strange', because there are positive exponents) underlies fluid motion on this computational domain. Coarsely resolved shear turbulence at this Reynolds number is describable, at least theoretically, by a finite number of degrees of freedom. However, this number is large enough to invalidate any notion that the global dynamics of this turbulent flow can be attributed to the interaction of a 'few' degrees of freedom.

The calculation of spectra at two different time steps for this spatial resolution was undertaken to determine the sensitivity of the spectra to such changes. Contrary to initial expectation, small differences did appear. Choice of a time step for integration in any particular turbulence simulation depends upon a combination of perceived algorithm stability limits and desired accuracy. However, because of the general complexity of such calculations, larger time steps are more likely to be chosen so that the maximum 'flow time' is obtained from the computational resources. In addition, the usually calculated means and second-order statistics of such simulations are frequently insensitive to time step changes over substantial ranges. This is certainly true here, where no significant or systematic differences between statistics of an individual $\Delta t u_\tau / L = 0.003$ simulation and those for the $\Delta t u_\tau / L = 0.0015$ case, partially displayed in §2, were detectable. There seems no reason under such circumstances to choose smaller steps. There is even less reason to choose smaller steps in an exponent calculation, given that many simultaneous simulations are

being performed, and computational resources are finite. However, as is obvious from figure 7, small but persistent differences between the Lyapunov exponent spectra of the two different time integrations were found. Some small part of them can be attributed to lack of convergence over these averaging times. In figure 8 the time history of the running average of λ_1, the first exponent calculated in each spectrum, is shown for integrations some six times longer than used to obtain exponents 1–63 in figure 7. While the difference between these two values does decrease, they remain distinct after averaging times corresponding to convection over $7435L$. Though integration at a larger time step may be regarded as a sort of filter on possible dynamics, power spectra from the two flows have few differences at high or low frequencies.

The explanation for the majority of these differences lies in the fact that the total dissipation of a discretely integrated dynamical system varies with the time step employed and that the dimension of the attractor is a sensitive indicator of this. The integration scheme maps the flow field at one instant to that $\Delta t u_\tau/L$ later. Changing Δt changes the discrete dissipation of this map. From the lack of variation in statistics it must be that substantially the same set of flow states is visited by the different integrations and with the same probability. However, the order in which these states is visited changes with different time steps. The Lyapunov exponents are a statistic characteristic of the *change* of the solution rather than the solution itself; perhaps then it is not surprising that a doubling of time step produces some change in exponent values. Just as many processes can have the same probability density with wildly differing dynamics, so also two flows with similar Reynolds stress distribution could have different Lyapunov exponents. Lyapunov exponents are statistics on the change from one flow state to the next; stress distributions are statistics on all the flow states visited, regardless of the order.

These effects can be demonstrated analytically using the Lorenz equations:

$$\left.\begin{aligned} \dot{X} &= \sigma(Y-X), \\ \dot{Y} &= \rho X - Y - XZ, \\ \dot{Z} &= -\beta Z + XY. \end{aligned}\right\} \tag{4.1}$$

The total dissipation ϵ per unit time of this system (equal to the trace of the Jacobian of (4.1)) is fixed at $-(\sigma+\beta+1)$. Use of the forward Euler scheme on this system produces a three-dimensional map whose Jacobian is

$$\boldsymbol{J} = \begin{bmatrix} 1-\sigma\Delta t & \sigma\Delta t & 0 \\ (\rho - Z_n)\Delta t & (1-\Delta t) & -X_n\Delta t \\ Y_n\Delta t & X_n\Delta t & (1-\beta\Delta t) \end{bmatrix}. \tag{4.2}$$

For a map the product of the eigenvalues of its Jacobian gives the net volumetric change per iteration, and the natural logarithm of the volumetric change, divided by Δt, gives the effective dissipation of the discrete dynamical system. Conveniently, the product of the eigenvalues turns out to be the determinant of $\boldsymbol{J}$, or

$$\begin{aligned} \det[\boldsymbol{J}] = 1-(\sigma+\beta+1)\Delta t + [\sigma(1-\beta-\rho+Z_n)+\beta+X_n^2]\Delta t^2 \\ + \sigma\Delta t^3[\beta(\rho-Z_n-1)-X_n(X_n+Y_n)], \end{aligned} \tag{4.3}$$

Expanding the logarithm of (4.3) for arguments near unity one finds that

$$\epsilon = -(\sigma+\beta+1) + O([Z_n, X_n^2]\Delta t) + O([X_n, Y_n, Z_n]\Delta t^2). \tag{4.4}$$

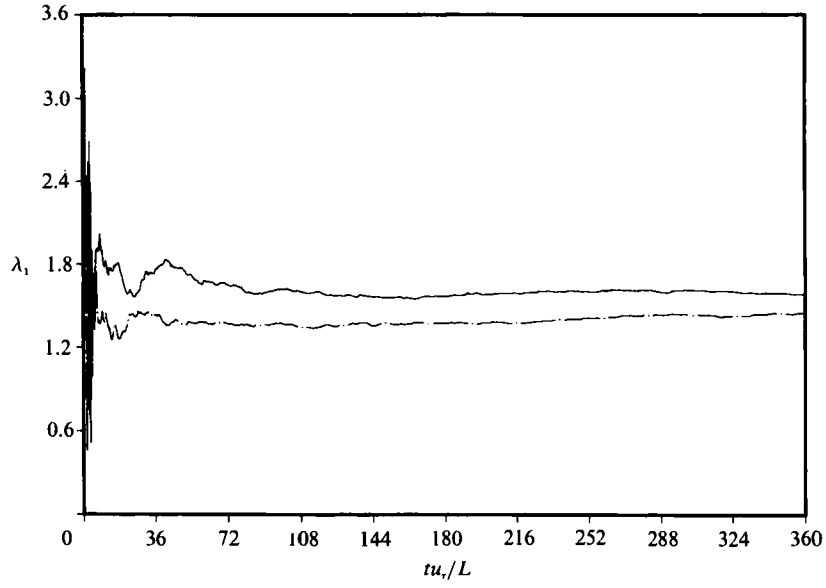

FIGURE 8. Time history of λ_1 for two different integration time steps: ———, 0.0015; —·—, 0.003.

Time step Δt	Averaging time	Dissipation, theory	Exponent sum
0.001	1000	−13.701 43	−13.701 45
0.002	1000	−13.734 84	−13.734 56
0.005	1000	−13.830 49	−13.828 10
0.01	1000	−13.955 53	−13.949 04
0.02	1000	−14.379 42	−14.402 33
0.023	1150	−14.478 07	−14.548 56

TABLE 3. Comparison of discrete dissipation and sum of Lyapunov exponents for the Lorenz equations integrated using forward Euler. $\rho = 28$, $\epsilon = -(\sigma+\beta+1) = -41/3 = -13.666\,666...$

As expected the discrete dissipation equals the analytic value when Δt approaches zero, but for realistic values of Δt below the stability limit of the integration scheme, ϵ varies macroscopically because X_n, etc. can be much larger than one. This can be seen in table 3, where the averaged discrete dissipation of the Lorenz system, integrated using forward Euler, is compared against the sum of its calculated exponents as Δt is varied. Note that the exponents in this calculation were obtained with the same technique as the channel flow calculation: the variational equations were not integrated, but rather a family of nearby initial conditions in phase space. This table confirms the earlier statement that a good algorithm estimates exponents consistent with the dissipation of the system, but that dissipation varies with integration time step.

The actual time integration scheme used to integrate the Navier–Stokes equations was more complicated, and more accurate, than forward Euler. At each of three substeps the nonlinear terms were advanced similar to forward Euler, while the viscous terms were advanced implicitly using Crank–Nicholson. The Lorenz system was also integrated using this scheme and the sum of its exponents calculated as Δt was varied. Table 4 displays the results. The higher accuracy of the scheme is

Time step Δt	Averaging time	Exponent sum
0.001	1000	−13.666 96
0.002	1000	−13.667 54
0.005	1000	−13.671 80
0.01	1000	−13.687 98
0.02	1000	−13.760 29
0.023	1150	−13.792 34
0.05	1000	−14.406 25

TABLE 4. Sum of Lyapunov exponents for the Lorenz equations integrated with Runge–Kutta–Wray/Crank–Nicholson scheme. $\rho = 28$, $\epsilon = -(\sigma+\beta+1) = -41.3 = -13.666\,666...$

reflected in the decreased variation of the calculated sum; here only a 1% variation in dissipation occurs within what would be the linearly stable range of the explicit advance, while 5% occurs for larger but implicitly stable Δt.

The effects of a dissipation change on the calculated dimension can be derived from a simple model. The Lyapunov exponent distribution is discrete:

$$\lambda_n = \lambda_1 - b(n-1)^r, \quad \lambda_1, b, r > 0, \quad n = 1, 2, 3..., \tag{4.5}$$

but for analytic ease consider n continuous. The exponent r lies in the range $\frac{1}{2} \leqslant r \leqslant \frac{2}{3}$ in our channel flow calculations. Now define a summation (integration) function

$$S(M) = \int_1^M \lambda_n \, \mathrm{d}n = \lambda_1(M-1) - \frac{b(M-1)^{r+1}}{r+1}. \tag{4.6}$$

Then the Lyapunov dimension, D_λ, and the total dissipation ϵ (for a system with Q exponents) are defined by

$$S(D_\lambda) = 0, \quad S(Q) = \epsilon, \tag{4.7a, b}$$

Solve (4.7a) for a relation between D_λ and λ_1 ($D_\lambda \gg 1$):

$$D_\lambda = \left[\frac{(r+1)\lambda_1}{b}\right]^{1/r}, \tag{4.8}$$

and logarithmically differentiate with respect to λ_1 (r, b constant) to obtain

$$\frac{\mathrm{d}D_\lambda}{D_\lambda} = \frac{1}{r}\frac{\mathrm{d}\lambda_1}{\lambda_1}. \tag{4.9}$$

In a similar fashion, for $Q \gg 1$, write (4.7b) as a relation between ϵ and λ_1 and logarithmically differentiate to obtain

$$\left[1 - \frac{bQ^r}{\lambda_1(r+1)}\right]\frac{\mathrm{d}\epsilon}{\epsilon} = \frac{\mathrm{d}\lambda_1}{\lambda_1}. \tag{4.10}$$

Combining (4.9) and (4.10, using the experimental spectrum for values of λ_1/b, and assuming $Q = 6930$ and $\frac{1}{2} \leqslant r \leqslant \frac{2}{3}$ gives that

$$[-8.85, -6.8] \times \frac{\mathrm{d}\epsilon}{\epsilon} = \frac{\mathrm{d}D_\lambda}{D_\lambda}. \tag{4.11}$$

Thus within the spectrum shape assumption of the model, small changes in the dissipation express themselves as amplified variations of λ_1 and still greater variation

of the dimension D_λ. When $r = \frac{2}{3}$ a 1% change in ϵ causes a 5.9% change in λ_1 and a 8.85% change in D_λ. Working backwards from the calculated dimensions of 352 and 308, this 12.5% decrease when the time step doubled could easily result from only a 1.5% change in dissipation. We emphasize that an exponent and dimension calculation are peculiarly sensitive to these effects of global dissipation change and that none of the usual turbulence statistics are affected.

In addition to revealing the asymptotic differences between the two spectra at different time steps figure 8 illustrates the slow convergence of the low-indexed exponents. In a theoretical analysis of the general behaviour of Lyapunov exponents in finite-dimensional systems, Goldhirsch, Sulem & Orszag (1987), argued that a t^{-1} convergence to the average was to be expected. Such behaviour was confirmed to occur in several low-order dynamical systems (Lorenz, Mackay–Glass, Rabinovich–Fabrikant, Curry, Knobloch–Weiss) and a method for extrapolation of these running averages to $t = \infty$ suggested and successfully demonstrated as a way to decrease total calculation time. No similar reduction in calculation time was achieved by applying this technique here. The method consists of obtaining a least-squares fit of an exponent's running average to an expression of the form $\lambda_i(t) = b_i + (a_i/t)$. The value of b_i obtained from the fit is the asymptotic value of the exponent. In our calculations the length of low-index-exponent time history required to obtain a stable estimate of the b_i differed little from the time needed for the exponent to converge. For the high-index exponents convergence of the average was so rapid that extrapolation was unnecessary. Similar problems in extrapolation were found by Vastano & Moser (1991) in exponent calculations of Taylor–Couette flow near the turbulent transition, but Sirovich & Deane (1991) employed the method successfully in their exponent calculations in Bénard convection. Problems in extrapolation appear to be associated with the substantial variability of the local exponents from one orthonormalization to the next in the two shear flow cases. Time histories of exponents in Bénard convection are much smoother.

Aside from the basic ability to accurately integrate the Navier–Stokes equations in time for the channel flow, the other crucial component of the exponent algorithm is the repeated orthonormalization of separation vectors between the base flow and the perturbations. The Gram–Schmidt procedure is well known to be ill-conditioned under certain circumstances, and gets progressively worse as the number of mutually orthogonal vectors sought increases. Less ill-conditioned is the modified Gram–Schmidt procedure used here, but ultimately the only way to check for independence is to construct inner products between each pair of vectors. Since the orthogonalization was conducted in single-precision (64-bit) arithmetic, the inner product must be calculated in double precision to be a true indicator. Such an operation was performed at 52 evenly spaced intervals in the $\Delta t u_\tau / L = 0.0015$ calculation during the time that all 450 exponents were being calculated. At each interval the $\frac{1}{2}(450 \times 449) = 101\,025$ possible normalized inner products between all pairs of vectors were calculated. The 5.25 million numbers so obtained are histogrammed in figure 9. The maximum value of any normalized inner product (cosine of the angle between vectors) during the entire interval was less than 2^{-35} (3×10^{-11}), with 84% of the values less than 2^{-39} (2×10^{-12}), While these values are not machine zero they are small enough to erase any doubts that the modified Gram–Schmidt procedure used in the orthogonalization was inadequate to the task. It should be remembered that the dimension of the vector space in which the orthogonalization occurred was 6930. The 450 vectors span only 6.5% of the possible directions in this space. Thus if one ignores a certain accumulation of round-off error as the absolute number of

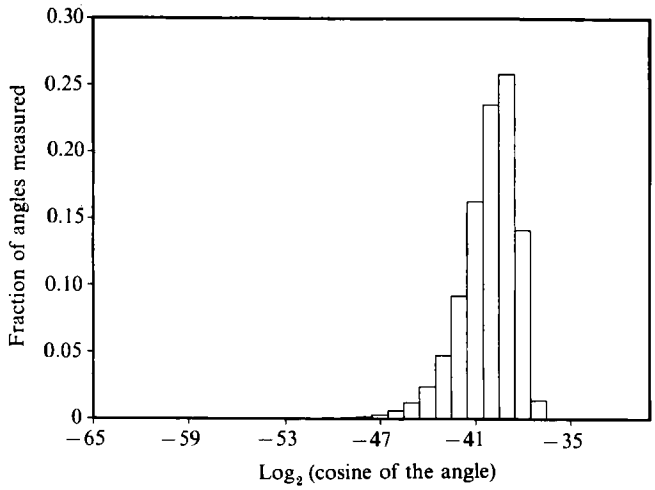

FIGURE 9. Lyapunov vector orthogonality statistics obtained from the 450 exponent calculation using $\Delta t u_\tau / L = 0.0015$

vectors increases, orthogonalizing 450 vectors out of 6930 should present no more problems than 2 out of 32, and this latter hardly seems a formidable task.

4.2. *Medium and high spatial resolution*

Finite computational resources balanced against the number of simultaneous flow simulations required to obtain the dimension estimates described in the previous section mandated that each simulation be coarse grained spatially. As shown in §3 the statistics of such simulations (stress, turbulence intensity, and velocity profiles) display some departures from those of experiments and more highly resolved simulations (Kim *et al.* 1987) at similar, though higher, Reynolds numbers. Such departures in statistics are often taken to indicate that the flow being simulated is not 'true' turbulence. On the other hand, wavenumber spectra and distributions calculated on higher-resolution grids ($16 \times 33 \times 16$ and $32 \times 33 \times 32$) in this spatial domain fare better in such comparisons. What are the corresponding changes in the Lyapunov exponent spectra and Kaplan–Yorke dimension as more lengthscales are included and 'true' turbulence is approached. Does the dimension go up or down? Does its value asymptote as resolution increases? Unless this latter question can be answered affirmatively, the 'finiteness' of the attractor dimension calculated will be completely spurious. To answer these questions, exponent calculations were performed at the two higher spatial resolutions. In neither case did we obtain sufficient numbers of exponents to apply the Kaplan–Yorke formula directly. However, in the medium-resolution case we calculated all the positive exponents, and they confirmed a scaling relation for spectrum shape versus resolution that allowed us to estimate the dimension at this and higher resolutions when only part of the exponent spectrum is available.

In two previous studies of chaotic solutions to partial differential equations (Manneville 1975; Keefe 1989), as well as one study of a large system of ordinary differential equations (Yamada & Ohkitani 1988) the investigators found that the Lyapunov exponent spectra of each system were collapsed by normalization of the exponent values by the ratio $N_{\geqslant}/h_\mu$, and their indices by $1/N_{\geqslant}$. Here $N_{\geqslant}$ is the number of non-negative exponents, and h_μ (an upper bound on the metric entropy) equals the sum of these exponents. In each case, this scaling was observed as a

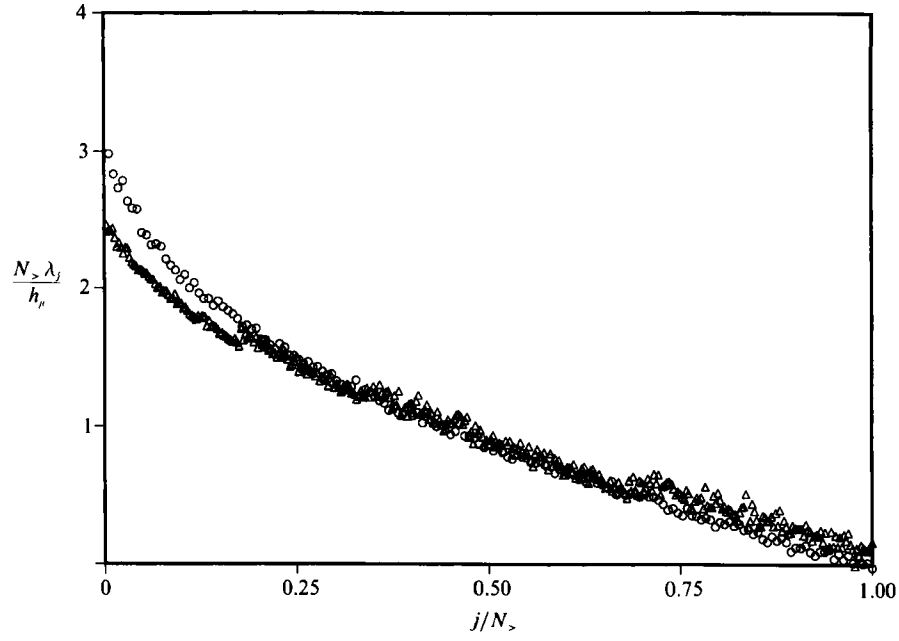

FIGURE 10. Normalized Lyapunov exponent spectra from coarse (○), and medium (△) resolution calculations.

control parameter in the equations (effectively, the Reynolds number) became large, and the number of computational modes in the calculation increased. Related to this same scaling is the use by Sirovich & Deane (1991) of a linear extrapolation technique to estimate the attractor dimension in Bénard convection when sufficient exponents could not be calculated.

This same scaling was found to hold here where the Reynolds number was fixed, but the number of computational modes was doubled. On a $16 \times 33 \times 16$ grid the first 380 exponents were calculated. This number was judged just sufficient for the values of λ_i to become negative, and we estimate $N_\geqslant = 368$. Figure 10 shows this partial spectrum, along with the first 166 exponents of the coarse-grained case plotted in normalized form. Except for some differences below $j/N < \sim 0.15$, which are in part attributable to incompletely converged exponents in the medium-resolution case, the two normalized spectra are the same. Given the shape similarity of normalized spectra, the attractor dimension is proportional to the number of positive exponents. Thus for this medium resolution calculation we estimate $D_\lambda \sim (\frac{368}{166}) \times 352 \sim 780$. Doubling the spanwise resolution of the simulation has more than doubled the dimension of the underlying attractor. One additional exponent spectrum, at still higher resolution, was obtained in an effort to determine if further dimension increases occur. In this case, we calculated estimates of the first 63 exponents from a $32 \times 33 \times 32$ simulation. Figure 11 shows these exponents, along with their counterparts from the medium- and coarse-grained simulations, in unscaled form. Because of the small number of exponents calculated at this highest resolution, and their scatter due to incomplete convergence, we cannot make a strong statement that the dimension does not increase again. However, our experience watching the other exponent spectra converge over long calculation times certainly convinces us such an increase could only be small. Even incompletely converged, the high-resolution spectrum pictured in the figure is parallel to, and tending towards coincidence with,

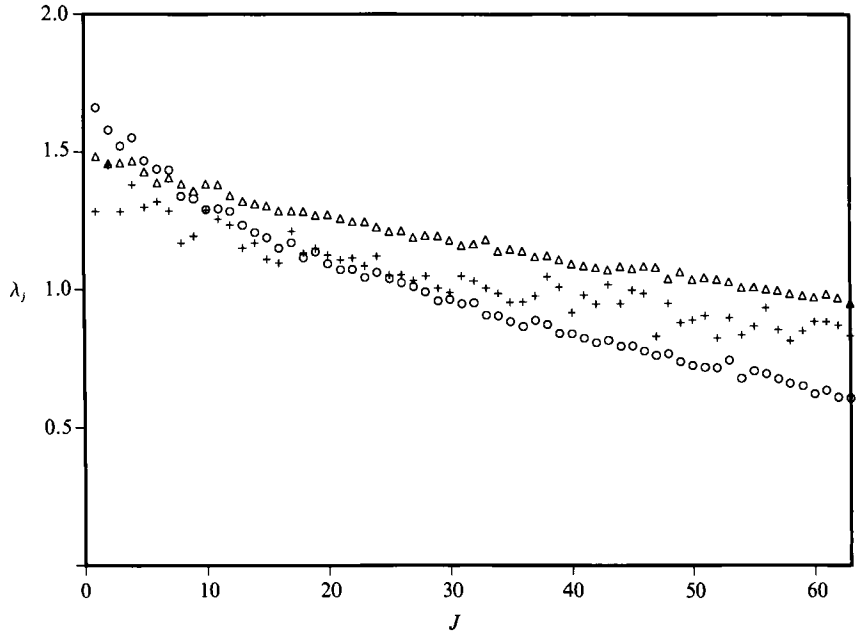

FIGURE 11. Unnormalized Lyapunov exponent spectra from the three different resolution calculations: ○, $16 \times 33 \times 8$; △, $16 \times 33 \times 16$; +, $32 \times 33 \times 32$.

the medium-resolution spectrum. Given the shape similarity of spectra, this is indicative, though weak, evidence that the attractor dimension asymptotes to value near $D_\lambda = 780$. If such near coincidence of the exponents were to be demonstrated for larger sections of the spectra, this last statement would be made conclusive. Unfortunately the task of calculating the estimated 400 non-negative exponents at high resolution needed to resolve this question is beyond reasonable computation at this time. We are confident that the attractor dimension on this computational domain is at least $D_\lambda = 780$; the evidence available suggests to us that its asymptotic value for a completely resolved turbulent flow is not much greater.

4.3. *Predictions for the spectrum shape*

Very little can be predicted about the shape of the Lyapunov exponent spectrum for an arbitrary dynamical system. However, we know of two such predictions for the Navier–Stokes equations. The first, due to Ruelle (1982), concerns the shape of the spectrum near $\lambda_j = 0$; the second, due to Constantin, Foias & Temam (1985), concerns its asymptotic shape for $j \to \infty$.

Ruelle's work predicts the possibility that the exponent distribution is tangent to the line $\lambda_j = 0$, provided the β-model of Frisch, Sulem & Nelkin (1978) is assumed for the dissipation ϵ. The β-model assumes ϵ to have its support on a fractal set of dimension α; there is now evidence from experiments (Meneveau & Sreenivasan 1987) and numerical calculation (Keefe & Deane 1989; Hosokawa & Yamamoto 1990) that ϵ is a multifractal, finding support on a continuous distribution of fractal sets of varying dimension. The modifications to Ruelle's analysis needed to include these new data have not been made. It can be seen from the exponent spectra in figure 7 that the exponent distribution in low-Reynolds-number Poiseuille flow does not have a tangency at the prescribed place.

Constantin *et al.* (1985) predict the asymptotic shape of the exponent distribution

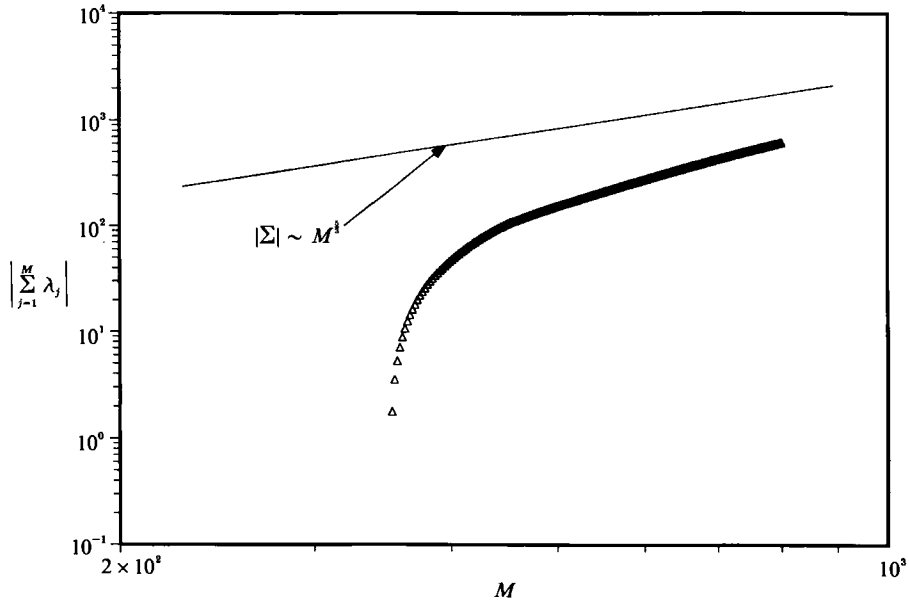

FIGURE 12. Summation of first $M = 800$ exponents, coarse-grained simulation, compared to predicted $M^{\frac{5}{3}}$ behaviour for large numbers of exponents.

by an argument based on bounds to the distribution of the eigenvalues of the Stokes operator in the Navier–Stokes equation. Shorn of the various technical arguments that lead up to it, this prediction takes the form

$$\left|\sum_{j=1}^{M}\lambda_j\right| \geqslant C_1 M^{\frac{5}{3}} \quad (M \text{ large}). \tag{4.12}$$

To test the exponent spectra against this bound we returned to the coarse-grained simulation and added an additional 350 exponents to the calculation, obtaining estimates of the first 800 exponents. The absolute value of the sum of exponents is plotted in figure 12 on log-log axes along with a line that corresponds to $M^{\frac{5}{3}}$ behaviour. It first must be said that $M = 800$ does not apparently constitute a large enough index for true asymptotic behaviour to appear. However, that part of the exponent distribution that is available does not violate the bound, and is tending towards the predicted behaviour.

5. Implications of these results

The results described above have important implications for many current studies of fluid turbulence. Foremost, we believe that we have supplied strong evidence that solutions to the Navier–Stokes equations for turbulent channel flow are confirmed to a finite-dimensional strange attractor, and thus temporal chaos in this representative shear flow results from the 'sensitive dependence' mechanism intrinsic to such attractors. This suggests a new mathematical context for turbulence studies, different from the Reynolds-averaged and statistical approaches. The structure of turbulence now means not only its visible, three-dimensional manifestation, but also the largely obscure, higher-dimensional fractal structure of its underlying attractor. It is in this latter context that the unpredictability of turbulent flow, as well as its approximate recurrent structure in time and space can now be understood as the

result of a competition, never resolved, between ubiquitous local instability and global boundedness. These are new insights, inaccessible from previous methods of study.

Though the dimension of the attractor in the current study is finite, its magnitude places this dynamical system in an entirely different class from those analysed experimentally in the Bénard or Taylor–Couette problems. For experimentalists the news is largely negative, for no available method of calculating dimension from measured data can handle a dimension so high. The number of points required for the 'correlation' dimension, if the scaling region is to extend over only a factor of 2, is 10^{234}! A billion points would give a scaling region within a radius variation of only 3%. Thus there was no chance that the previous attempts to calculate dimension by these methods could have succeeded. For those seeking a simplification of the turbulence problem by decomposing the flow onto special bases the resultant dynamical system is still likely to be too complex for analysis. Simply extracting the fixed points of a 780th-order system is a non-trivial task, and the subsequent analysis of phase-space orbits in terms of these singularities is daunting even to contemplate. Thus it seems unlikely, given the dimension of the attractor, that even a 100-mode truncation could get the basic, qualitative dynamics of the full system correct. Under these conditions a more local approach to decomposition (Lumley 1981; Aubry *et al.* 1988) seems to hold promise.

Dynamical systems theory has provided the tools and arguments to demonstrate that turbulence is finite-dimensional. This dimension is large, but not infinite. The infinite can induce an intellectual paralysis that may discourage the search for new analysis techniques. Our demonstration that a well-known shear flow has finite degrees of freedom should help to dissipate this paralysis. Others have long since embraced these notions and staked out new territory in the study of finite-dimensional reductions of formally infinite-dimensional systems (Sirovich & Rodriguez 1987; Aubry *et al.* 1988; Foias *et al.* 1988; Kevrekidis, Nicolaenko & Scovel 1990; Rodriguez & Sirovich 1990). The older Karhunen–Loéve approach has recently been linked to the newer study of inertial manifolds. Sirovich, Knight & Rodriguez (1990) have shown that the calculation of an approximate inertial manifold for a p.d.e. is equivalent to performing the Karhunen–Loéve procedure on the time derivative of its solution, rather than on the solution itself. The usual Karhunen–Loéve procedure produces a basis set that optimally captures the mean-square projection of the amplitude of the system; calculating an approximate inertial manifold produces a basis set that optimally captures the mean-square projection of the time derivative. In at least one example it has been shown that for similar accuracy in describing the bifurcation structure and dynamics of the solution the latter approach produces a smaller set of differential equations than the traditional approach. Our results should encourage the further application of these techniques to the Navier–Stokes equations.

6. Conclusions

Using numerical simulations to calculate Lyapunov exponent spectra, the dimension of the strange attractor underlying periodic, fully developed, turbulent Poiseuille flow at a pressure-gradient Reynolds number of 3200 on a particular computational domain has been estimated to be $D_\lambda \sim 780$. A spatially coarse-grained calculation ($16 \times 33 \times 8$) established a lower bound of $D_\lambda \sim 352$. In this simulation sufficient of the Lyapunov spectrum was calculated for a direct application of the

Kaplan–Yorke formula for dimension. At medium spatial resolution ($16 \times 33 \times 16$) the full spectrum necessary for application of the Kaplan–Yorke formula could not be obtained owing to computational constraints. However, a calculation of the non-negative exponents (some 368 of them) showed that Lyapunov spectra display a universal shape in this flow, as resolution increases, when normalized using the number of non-negative exponents $N_{\geqslant}$ and the metric entropy, h_{μ}. On this basis the dimension of the underlying attractor was estimated to be $D_{\lambda} \sim 780$ at the medium resolution. A small segment of exponent spectra calculated when streamwise and spanwise resolutions were further doubled ($32 \times 33 \times 32$) supports the contention that the asymptotic value of the dimension in fully resolved turbulence is not likely to be much larger.

These results demonstrate that fully developed channel flow is deterministic chaos confined to a strange attractor, and that temporal unpredictability in this representative bounded shear flow is due to the exponential spreading property integral to such attractors. The magnitude of the estimated dimension destroys any possibility that the global dynamics of this fully developed flow can be attributed to the interaction of 'a few degrees of freedom'. This distinguishes Poiseuille flow from either Bénard convection or Taylor–Couette flow.

A switch to a new mathematical context for studies of fully developed turbulence is supported by these results, one that is quite separate from the Reynolds-averaged or statistical viewpoints. The linear methodology of Fourier transformations inherent in the latter has provided many insights into turbulence phenomena in the last half century, but only the nonlinear viewpoint, objectified in the strange attractor, could suggest the mechanism and origin of temporal disorder, the feature that has made the averaged and statistical points of view a necessity until now. The new viewpoint is a geometrical one, but forces us to think in spaces of dimension greater than a comfortable three, where entire flow fields are represented by a single point. Such a shift in thinking will not be easy. However, the potential benefit seems large. The physical phenomena of turbulence must find echo or origin in the mathematical structure of its underlying attractor. The study of the mathematical properties of these attractors should provide not only a framework for what we already know but predict things we do not.

During the course of this work the first author has received support from the National Research Council, the Air Force Office of Scientific Research (Contract AFOSR 88-056), and the NASA-Ames/Stanford University Center for Turbulence Research. The grant of substantial blocks of computer time from both the NASA-Ames Research Center and the Numerical Aerodynamic-Simulation program (NAS) is also gratefully acknowledged.

REFERENCES

ABERGEL, F. 1990 Attractor for a Navier–Stokes flow in an unbounded domain. *Modél. Math. Anal. Numér.* **23**, 359–370.

AUBRY, N., HOLMES, P., LUMLEY, J. L. & STONE, E. 1988 The dynamics of coherent structures in the wall region of a turbulent boundary layer. *J. Fluid Mech.* **192**, 115–174.

BENETTIN, G., GALGANI, L., GIORGILLI, A. & STRELCYN, J.-M. 1980 Lyapunov exponents for smooth dynamical systems; A method for computing all of them. Part 2: Numerical application. *Meccanica* **15**, 21–30.

BRANDSTADTER, A. & SWINNEY, H. L. 1987 Strange attractors in weakly turbulent Couette–Taylor flow. *Phys. Rev.* A **35** 2207–2220.

BRANDSTADTER, A., SWINNEY, H. L. & CHAPMAN, G. T. 1986 Characterizing turbulent channel flow. In *Entropies and Dimensions in Chaotic Systems* (ed. G. Mayer-Kress). Springer.

BROOMHEAD, D. S. & KING, G. P. 1986 On the qualitative analysis of experimental dynamical systems. In *Nonlinear Phenomena and Chaos* (ed. S. Sarkar). Adam Hilger.

BUSSE, F. H. 1981 Transition to turbulence in Rayleigh–Bénard convection. In *Hydrodynamic Instabilities and the Transition to Turbulence* (ed. H. L. Swinney & P. J. Gollub), pp. 97–137. Springer.

CONSTANTIN, P. & FOIAS, C. 1985 Global Lyapunov exponents, Kaplan–Yorke formulas and the dimension of the attractors for 2D Navier–Stokes equations. *Commun. Pure Appl. Maths.* **38**, 1–28.

CONSTANTIN, P., FOIAS, C. & TEMAM, R. 1985 Attractors representing turbulent flows. *Mem. Am. Maths. Soc.* **53**, no. 314.

CURRY, J. H., HERRING, J. R., LONCARIC, J. & ORSZAG, S. A. 1984 Order and disorder in two-and three-dimensional Bénard convection. *J. Fluid Mech.* **147**, 1–38.

ECKELMANN, H. 1974 The structure of the viscous sublayer and the adjacent wall region in turbulent channel flow. *J. Fluid Mech.* **65**, 439–459.

ECKMANN, J.-P. & RUELLE, D. 1985 Ergodic theory of chaos and strange attractors. *Rev. Mod. Phys.* **57**, 617–650.

FARMER, J. D. 1982 Chaotic attractors of an infinite dimensional system. *Physica* **4D**, 366–393.

FARMER, J. D., OTT, E. & YORKE, J. A. 1983 The dimension of chaotic attractors. *Physica* **7D**, 153–180.

FOIAS, C., JOLLY, M. S., KEVREKIDIS, I. G., SELL, G. R. & TITI, E. S. 1988 On the computation of inertial manifolds. *Phys. Lett.* A **131**, 433–436.

FOIAS, C. & TEMAM, R. 1984 Determination of the solutions of the Navier–Stokes equations by a set of nodal values. *Maths Comput.* **43**, 117–133.

FREDERICKSON, P., KAPLAN, J. L., YORKE, E. D. & YORKE, J. A. 1983 The Lyapunov dimension of strange attractors. *J. Diffl Equat.* **49**, 185–207.

FRISCH, U., SULEM, P.-L. & NELKIN, M. 1978 A simple dynamical model of intermittent fully developed turbulence. *J. Fluid Mech.* **87**, 719–736.

GOLDHIRSCH, I., SULEM, P.-L. & ORSZAG, S. 1987 Stability and Lyapunov stability of dynamical systems: a differential approach and a numerical method. *Physica* **27D**, 311–337.

GOLLUB, J. P. & BENSON, S. V. 1980 Many routes to turbulent convection. *J. Fluid Mech.* **100**, 449–479.

GORMAN, M., WIDMANN, P. J. & ROBBINS, K. A. 1986 Nonlinear dynamics of a convection loop: A quantitative comparison of experiment and theory. *Physica* **19D**, 253–267.

GRAPPIN, R. & LÉORAT, J. 1991 Lyapunov exponents and the dimension of periodic incompressible Navier–Stokes flows: numerical measurements. *J. Fluid Mech.* **222**, 61–94.

GRASSBERGER, P. & PROCACCIA, I. 1983 Measuring the strangeness of strange attractors. *Physica* **9D**, 189–208.

HERBERT, TH. 1977 Finite amplitude stability of plane parallel flows. *AGARD CP*-224, pp. 3.1–3.10.

HOSOKAWA, I. & YAMAMOTO, K. 1990 Intermittency exponents and generalized dimensions of directly simulated fully developed turbulence. *Phys. Fluids* A **2**, 889–892.

HUERRE, P. & MONKEWITZ, P. 1985 Absolute and convective instabilities in free shear layers. *J. Fluid Mech.* **159**, 151–168.

JIMINEZ, J. & MOIN, P. 1991 The minimal flow unit in near-wall turbulence. *J. Fluid Mech.* **225**, 213–240.

KEEFE, L. R. 1985 Dynamics of perturbed wavetrain solutions to the Ginzburg–Landau equation. *Stud. Appl. Maths* **73**, 91–153.

KEEFE, L. 1989 Properties of Ginzburg–Landau attractors associated with their Lyapunov vectors and spectra. *Phys. Lett.* A **140**, 317–322.

KEEFE, L. & DEANE, A. E. 1989 Multifractal spectra in shear flows. In *Proc. 7th Symp. on Turbulent Shear Flows, Stanford University, August 1989*, Paper 30-3.

KEEFE, L., MOIN, P. & KIM, J. 1990 Applications of chaos theory to shear turbulence. In *The*

Ubiquity of Chaos (ed. S. Krasner), pp. 56–63. American Association for the Advancement of Science.

KEVREKIDIS, I. G., NICOLAENKO, B. & SCOVEL, J. C. 1990 Back in the saddle again: A computer assisted study of the Kuramoto–Sivashinsky equation. *SIAM J. Appl. Maths* **50**, 760–790.

KIM, J., MOIN, P. & MOSER, R. 1987 Turbulence statistics in fully developed channel flow at low Reynolds number. *J. Fluid Mech.* **177**, 133–166.

LIBCHABER, A., FAUVE, & LAROCHE, C. 1983 Two parameter study of the routes to chaos. *Physica* **7D**, 73–84.

LUMLEY, J. L. 1981 Coherent structures in turbulence. In *Transition and Turbulence* (ed. R. Meyer), pp. 215–242. Academic.

MANNEVILLE, P. 1985 Lyapunov exponents for the Kuramoto–Sivashinsky model. *Conf. on Macroscopic Modelling of Turbulent Flows*. Lecture Notes in Physics, vol. 230, p. 319. Springer.

MENEVEAU, C. & SREENIVASAN, K. 1987 The multifractal spectrum of the dissipation field in turbulent flows. *Nucl. Phys.* B (*Proc. Suppl*) **2**, 49–76.

MOIN, P. & MOSER, R. D. 1989 Characteristic-eddy decomposition of turbulence in a channel. *J. Fluid Mech.* **200**, 471–510.

MOORE, D. R., TOOMRE, J., KNOBLOCH, E. & WEISS, N. O. 1983 Period doubling and chaos in partial differential equations for thermosolutal convection. *Nature* **303**, 643–647.

ORSZAG, S. 1971 Accurate solution of the Orr–Sommerfeld stability equation. *J. Fluid Mech.* **50**, 689–703.

OSLEDEC, V. I. 1968 A multiplicative ergodic theorem. Lyapunov characteristic numbers for dynamical systems. *Trans. Moscow Math. Soc.* **19**, 197.

PLATT, N., SIROVICH, L. & FITZMAURICE, N. 1991 An investigation of chaotic Kolmogorov flows. *Phys. Fluids* A **3**, 681–696.

PRASAD, R. R., MENEVEAU, C. & SREENIVASAN, K. R. 1988 Multifractal nature of the dissipation field of passive scalars in turbulent flows. *Phys. Rev. Lett.* **61**, 74–77.

RUELLE, D. 1982 Large volume limit of the distribution of characteristic exponents in turbulence. *Commun. Math. Phys.* **87**, 287–302.

RODRIGUEZ, J. D. & SIROVICH, L. 1990 Low dimensional dynamics for the complex Ginzburg–Landau equation. *Physica* **43D**, 77–86.

ROZHDESTVENSKY, B. L. & SIMAKIN, I. N. 1984 Secondary flows in a plane channel: their relationship and comparison with turbulent flows. *J. Fluid Mech.* **147**, 261–289.

SHIMADA, I. & NAGASHIMA, T. 1979 A numerical approach to ergodic problem of dissipative dynamical systems. *Prog. Theor. Phys.* **61**, 1605–1615.

SIEBER, M. 1987 Experiments on the attractor dimension of turbulent pipe flow. *Phys. Lett.* A **122**, 467–470.

SIROVICH, L., BALL, K. S. & KEEFE, L. 1990 Plane waves and structures in turbulent channel flow. *Phys. Fluids* A **2**, 2217–2226.

SIROVICH, L. & DEANE, A. 1991 A computational study of Rayleigh–Bénard convection. Part 2. Dimension considerations. *J. Fluid Mech.* **222**, 251–266.

SIROVICH, L., KNIGHT, B. W. & RODRIGUEZ, J. D. 1990 Optimal low-dimensional dynamical approximations. *Q. Appl. Maths* **48**, 535–548.

SIROVICH, L. & RODRIGUEZ, J. D. 1987 Coherent structures and chaos: A model problem. *Phys. Lett.* A **120**, 211–214.

SIROVICH, L., RODRIGUEZ, J. D. & KNIGHT, B. W. 1990 Two boundary value problems for the Ginzburg–Landau equation. *Physica* **43D**, 63–76.

VASTANO, J. A. & MOSER, R. D. 1991 Short-time Lyapunov exponent analysis and the transition to chaos in Taylor–Couette flow. *J. Fluid Mech.* **233**, 83–118.

WOLF, A., SWINNEY, H., FRASER, A. & VASTANO, J. 1985 Determining Lyapunov exponents from time series. *Physica* **16D**, 285–317.

YAMADA, M. & OHKITANI, K. 1988 Lyapunov spectrum of a model of two-dimensional turbulence. *Phys. Rev. Lett.* **60**, 983–986.